Am J Transl Res 2021;13(7):8480-8495
www.ajtr.org /ISSN:1943-8141/AJTR0133032

Original Article

Exposure to methylphenidate during peri-adolescence decouples the prefrontal cortex: a multimodal MRI study

Jack L Demaree[1], Richard J Ortiz[2], Xuezhu Cai[1], Dipak Aggarwal[1], Ilakya Senthilkumar[1], Christopher Lawson[1], Praveen Kulkarni[1], Bruce S Cushing[2], Craig Ferris[1,3]

[1]Center for Translational NeuroImaging, Northeastern University, Boston, MA, USA; [2]Department of Biological Sciences, University of Texas at El Paso, El Paso, TX 79968, USA; [3]Psychology and Pharmaceutical Sciences Northeastern University, Boston, MA, USA

Received March 11, 2021; Accepted May 26, 2021; Epub July 15, 2021; Published July 30, 2021

Abstract: This study was designed to assess the effects of daily psychostimulant exposure during juvenility and peri-adolescence on brain morphology and functional connectivity using multimodal magnetic resonance imaging. We hypothesized that long-term exposure to methylphenidate would enhance connectivity with the prefrontal cortex. Male rats were given daily injections of either methylphenidate (n=10), dextroamphetamine (n=10) or saline vehicle (n=10) from postnatal day 21 to 42. They were imaged between postnatal day 43 and 48. Voxel-based morphometry, diffusion weighted imaging, and resting state functional connectivity were used to quantify brain structure and function. Images from each modality were registered and analyzed, using a 3D MRI rat atlas providing site-specific data over 171 different brain areas. Following imaging, rats were tested for cognitive function using novel object preference. Long-lasting psychostimulant treatment was associated with only a few significant changes in brain volume and measures of anisotropy compared to vehicle. Resting state functional connectivity imaging revealed decreased coupling between the prefrontal cortex, basal ganglia and sensory motor cortices. There were no significant differences between experimental groups for cognitive behavior. In this exploratory study, we showed that chronic psychostimulant treatment throughout juvenility and preadolescence has a minimal effect on brain volume and gray matter microarchitecture, but significantly uncouples the connectivity in the cerebral/basal ganglia circuitry.

Keywords: Dextroamphetamine, adolescent, ADHD, psychostimulants, Ritalin, Adderall, MRI, resting state functional connectivity, cerebellum

Introduction

Attention deficit hyperactivity disorder (ADHD) is a developmental brain disorder characterized by inattentive and/or impulsive behavioral symptoms [1]. In the United States alone, approximately 9.4% of children and adolescents, primarily boys, aged 4-17, were diagnosed as having clinical expression of ADHD. Of these, 62.0% were prescribed with medication for treatment [2]. Furthermore, the Center for Disease Control (CDC) has reported that the disorder is becoming more prevalent with a 21.8% increase in parent-reported cases between 2003 and 2007. The heterogenous prevalence of the disorder across cultures and the disproportionate number of males has raised concerns around misdiagnosis and the inappropriate use of medication [3-5]. These concerns relate to the developmental neurobiology critical for the emotional and cognitive transition from childhood through adolescence [6]. The human brain develops throughout adolescence and into early adulthood, marked by synaptic pruning, decreases in gray matter and increases in white matter, optimizing the functional connectivity of different brain areas, e.g. prefrontal cortex (PFC) and cerebellum [7].

The etiology of ADHD is unknown. Impaired brain maturation with abnormalities in dopaminergic and noradrenergic neurotransmission appears to underlie the disorder [8]. The use of psychostimulants, such as methylphenidate (MPH; e.g. Ritalin®) and amphetamine (AMP; e.g. Adderall®) commonly used to treat ADHD,

enhances dopamine (DA) and norepinephrine (NE) neurotransmission via reuptake inhibition [9, 10]. This mechanism is thought to improve cognitive function of the PFC, an area implicated in the symptomology of ADHD [9, 11-13]. The PFC is involved in working memory, response inhibition and attention allocation, and is one of the last brain regions to develop [14]. Children with ADHD show altered structure and function in the PFC as compared to age matched controls [11, 13].

There have been numerous longitudinal studies in rodents looking at the effects of chronic MPH exposure prior to and during adolescence. These studies have focused on the behavioral and neurobiological consequences of early exposure, specifically around issues of adult drug sensitivity and liability, and disorders in emotion and cognition. The findings show no evidence of risk for future drug abuse when exposure is limited to preadolescence (postnatal days 20-35) and low doses of MPH. Indeed, they show a decrease in the rewarding effects of cocaine [15, 16] and less response to natural rewards [17], although, adult animals do show signs of anxiety-like and aversive behavior. However, the effects of early MPH exposure differ across strains of rodents, are dose- and sex-dependent, and sensitive to the transition between pre-adolescence and adolescence [18-23]. Giving low doses during adolescence or higher doses in pre-adolescence increases drug seeking behaviors, impairs cognitive function and alters dopaminergic neurotransmission and activity of the PFC [19, 24-27]. It should be noted that, Soto and colleagues exposed peri-adolescent rhesus monkeys to low doses of oral MPH and AMP for 18 months and reported little or no effect on physiological or behavioral/cognitive development [28].

The present study was undertaken to explore the effects of early MPH exposure, the mostly commonly prescribed psychostimulant for treating ADHD [29], on neurodevelopment in rodents by using multimodal magnetic resonance imaging (MRI). Dextroamphetamine (AMP) was included as a positive control. A global perspective on changes in brain structure and function is possible when the data are registered to, and analyzed, using a 3D MRI rat atlas covering 171 different brain areas as reported here. MRI has been used extensively in the clinic to study the acute and chronic effects of MPH in ADHD [30-32]. Prospective, longitudinal studies are hampered by the absence of a control arm, i.e., MPH treatment in normal children. This is not an obstacle in preclinical studies, as we treated "normal" rats from postnatal day 21 to 42 with vehicle, MPH or AMP. Given the emphasis assigned to the importance of the PFC in early development, we hypothesized that chronic exposure to psychostimulants during preadolescence would affect the morphology and functional connectivity of this brain area. To our surprise, the PFC showed loss of functional connectivity with MPH and AMP.

Methods and materials

Animals

Male Sprague Dawley rats were obtained from Charles River Laboratories (Wilmington, Massachusetts, USA). Rats were housed two per cage, maintained on a 12:12 hour light-dark cycle with lights on at 07:00 hours and allowed access to food and water ad libitum. All rats were acquired and cared for in accordance with the guidelines published in the Guide for the Care and Use of Laboratory Animals (National Institutes of Health Publications No. 85-23, Revised 1985) and adhered to the National Institutes of Health and the American Association for Laboratory Animal Science guidelines. The protocols used in this study complied with the regulations of the Institutional Animal Care and Use Committee at the Northeastern University (Comprehensive fMRI in Rodents for Preclinical Drug Discovery, Protocol #20-0628R) and adhere to the ARRIVE guidelines for reporting *in vivo* experiments in animal research [33].

Treatment and testing schedule

Rats were randomly assigned to one of three treatment groups: MPH (n=10), AMP (n=10), or saline vehicle (n=10). All treatments began on postnatal day 21 (PND 21). At approximately the same time each morning (9:00-10:00 hrs), rats were given intraperitoneal injections of MPH (10 mg/kg), AMP (5 mg/kg) or saline vehicle in a volume of 500 µl each. The dose of MPH was taken from the literature reporting daily treatments ranging from 4 to 20 mg/kg body weight [16, 17, 21, 24, 34, 35]. The dose of AMP was taken from the literature reporting daily treatments ranging from 1 to 5 mg/kg

body weight [36-40]. Daily treatments lasted for 21 days, ending on PND 42. We used the developmental periods defined by Venkataraman et al., to guide the treatment and imaging schedule with P21-P30 defined as juvenile, P31-P39 as preadolescence, and P40-P50 as adolescence [26]. It is estimated that during this prepubescent period from P21 to P50, 3.3 rat-days is equal to one human year [41], a treatment period in rats that could be equated to over six years in humans. The concentrations of the drugs were adjusted to account for an increase in body weight during this period of development from juvenility to adolescence keeping the dose and volume of injections constant. Scanning began on PND 43, the day after cessation of treatment and lasted for five days. Behavioral testing began on PND 50.

Behavioral testing

The novel object preference task (NOP) was used to assess episodic learning and memory as previously described [42, 43]. The apparatus consisted of a black cube-shaped Plexiglass box (L: 60.9, W: 69.2, H: 70.5 cm) with no lid, indirectly illuminated with two 40 W incandescent bulbs. Animals were placed in the empty box (15 min) for acclimation on day one. On day two, for the familiar phase (5 min), animals were placed in the box with two identical objects arranged in diagonal corners, 5 cm from each wall. After a 90 min rest period in their home cage, animals were placed back in the box for the novel phase (3 min) with one of the familiar objects and a novel object.

All rats were video recorded and analyzed using manual methods by experimenters that were blind to treatment conditions and verified with automated scoring using ANY-maze® software (Stoelting, Wood Dale, IL, USA). GraphPad Prism version 6.0 (GraphPad Software, La Jolla, CA) was used for statistical analyses. One-sample t-test assessed differences from chance levels (i.e., =50%) of exploration in the NOP task, for each experimental group individually. Comparisons among groups were conducted using one-way analysis of variance (ANOVA) with a critical value of 0.05.

Neuroimaging

Imaging sessions were conducted using a Bruker Biospec 7.0T/20-cm USR horizontal magnet (Bruker, Billerica, MA, USA) and a 20-G/cm magnetic field gradient insert (ID=12 cm) capable of a 120-μs rise time. Radio frequency signals were sent and received with a quadrature volume coil built into the animal restrainer (Ekam Imaging, Boston, MA, USA). The design of the restraining system included a padded head support obviating the need for ear bars helping to reduce animal discomfort while minimizing motion artifact. All rats were imaged under 1% isoflurane while keeping a respiratory rate of 40-50/min.

Voxel-based morphometry analysis

Images were acquired using RARE sequence with TR/TE =3310/36 ms; matrix size 256×256×40, field of view =30×30 mm, spatial resolution 0.117×0.117×0.7 mm as previously described [44, 45]. The scan takes approximately 3 min. A 3D MRI Rat Brain Atlas© (2012 Ekam Solutions LLC, Boston, MA USA) was used to calculate brain volumes, and registered the standard structural rat template image onto high resolution T2-weighted images for each subject using a non-linear registration method implemented by Unix based software package Deformable Registration via Attribute Matching and Mutual-Saliency Weighting (DRAMMS; https://www.cbica.upenn.edu/sbia/ software/dramms/index.html). The atlas (image size 256×256×63) (H×W×D) was then warped from the standard space into the subject image space (image size 256×256×40) using the deformation obtained from the above step using nearest-neighbor interpolation method. In the volumetric analysis, each brain region was therefore segmented, and the volume values were extracted for 171 ROIs, calculated by multiplying unit volume of voxel in mm^3 by the number of voxels using an in-house MATLAB script. To account for different brain sizes, all ROI volumes were normalized by dividing each subject's ROI volume by their total brain volume [44-46]. Statistical differences in measures of volumes between experimental groups were determined using a nonparametric Kruskal Wallis multiple comparisons test (critical value set at <0.05) followed by post hoc analyses using a Wilcoxon rank-sum test for individual differences.

Diffusion weighted imaging-quantitative anisotropy

DWI was acquired with a 3D spin-echo echo-planar-imaging (3D-EPI) pulse sequence hav-

ing the following parameters: TR/TE =500/20 msec, eight EPI segments, and 10 non-collinear gradient directions with a single B-value shell at 1000 s/mm^2 and one image with a B-value of 0 s/mm^2 (referred to as B0) as previously described [45, 47, 48]. Geometrical parameters were: 48 coronal slices, each 0.313 mm thick (brain volume) and with in-plane resolution of 0.313×0.313 mm^2 (matrix size 96×96; FOV 30 mm^3). The imaging protocol was repeated two times for signal averaging. Each DWI acquisition took 45 min and the entire MRI protocol including the anatomy lasted about 90 min. There are numerous studies detailing the benefits of multi-shot EPI in BOLD imaging [49-53]. We avoided using single shot EPI because of its sever geometrical distortion at high field strengths (≥7T) and loss of effective spatial resolution as the readout period increases [49, 54, 55]. There is also the possibility of signal loss in single shot EPI due to accumulated magnetic susceptibility or field inhomogeneity [50].

DWI analysis was completed with MATLAB and MedINRIA (1.9.0; http://www-sop.inria.fr/asclepios/software/MedINRIA/index.php) software. Because sporadic excessive breathing during DWI acquisition can lead to significant image motion artifacts that are apparent only in the slices sampled when motion occurred, each image (for each slice and each gradient direction) was screened prior to DWI analysis. If we found motion in more than one direction that subject was eliminated from the analyses. No subjects were eliminated in this study. For statistical comparisons among rats, each brain volume was registered to the 3D MRI rat brain atlas allowing voxel- and region-based statistics. All image transformations and statistical analyses were carried out using the in-house EVA software (Ekam Solutions LLC, Boston MA). For each rat, the B0 image was co-registered with the MRI atlas using a 9-parameter affine transform. The co-registration parameters were then used to create a map file for each subject. The average value for each ROI was computed using map files for each of the DWI indices.

Statistical differences in measures of DWI between experimental groups were determined using a nonparametric Kruskal Wallis multiple comparisons test (critical value set at <0.05) followed by post hoc analyses using a Wilcoxon rank-sum test for individual differences. The formula below was used to account for false discovery from multiple comparisons.

$$P(i) \leqslant \frac{i}{v} \frac{q}{c(v)}$$

P(i) is the *P* value based on the t test analysis. The false-positive filter value q was set to 0.2 and the predetermined c(V) was set to unity [56]. The corrected probability is noted on each table.

Resting state BOLD functional connectivity

Scans were collected using a spin-echo triple-shot EPI sequence (imaging parameters: matrix size =96×96×20 (H×W×D), TR/TE =1000/15 msec, voxel size =0.312×0.312×1.2 mm, slice thickness =1.2 mm, with 200 repetitions, and time of acquisition =10 min. Benefits of multi-shot EPI in BOLD imaging are described previously [49-53]. We avoided using single shot EPI because of its severe geometrical distortion at high field strengths (≥7T) and loss of effective spatial resolution as the readout period increases [49, 54, 55]. There is also the possibility of signal loss in single shot EPI due to accumulated magnetic susceptibility or field inhomogeneity [50]. The anatomical fidelity of the EPI images and their registration to the rat 3D MRI atlas are shown in Supplementary Figure 1.

Preprocessing was accomplished by combining Analysis of Functional NeuroImages (AFNI_17.1.12, http://afni.nimh.nih.gov/afni/), FMRIB Software library (FSL, v5.0.9, http://fsl.fmrib.ox.ac.uk/fsl/), Deformable Registration via Attribute Matching and Mutual-Saliency Weighting (DRAMMS 1.4.1, https://www.cbica.upenn.edu/sbia/software/drams/index.html) and MATLAB (MathWorks, Natick, MA). Brain tissue masks for rsFC images were manually drawn using 3DSlicer (https://www.slicer.org/) and applied for skull-stripping. While FSL is routinely used in human studies to extract the brain, we find the algorithm is inadequate for rodent studies. Pre-defined cerebrospinal fluid (ventricles) and white matter regions were segmented based on the 3D MRI rat brain atlas. After registration, the averaged time-courses were extracted and normalized. If outliers (i.e., data corrupted by extensive motion) were detected in the dataset, the corresponding time points were recorded so that they could be

regressed out in a later step. Functional data were assessed for the presence of motion spikes. Any large motion spikes, if identified, were removed from the time-course signals. This motion censoring step was followed by slice timing correction from interleaved slice acquisition order. Head motion correction (six motion parameters) was carried out using the first volume as a reference image. We did not use framewise-displacement-based scrubbing commonly used in human imaging, a method that sums the absolute values of the derivatives of the six realignment parameters, to identify excessive head motion. Instead, motion censoring was achieved by AFNI 3dToutcount and outliers were defined as number of MAD (median absolute deviation) that is allowed. The output contains the fraction of voxels per volume (within the automask) that exceeds the outlier limits after 3rd degree Legendre polynomial detrending. These time points are fed into AFNI 3dDeconvolve for nuisance regression.

Normalization was completed by registering functional data to the 3D MRI rat brain atlas using affine registration through DRAMMS [43, 48, 57]. The same atlas was used for segmentation into 171 brain areas. Data are reported in 166 brain areas only, as five regions in the brain atlas were excluded from analysis due to the large size of 3 brains. These brains fell slightly outside our imaging field of view and thus we did not get any signal from the extreme caudal tip of the cerebellum. Whole brains that contain all regions of interest are needed for analyses so rather than excluding the animals, we removed the brain sites across all animals. Nonlinear registration was performed to register individual images to standard rat brain template. Then, regressors comprised of demeaned motion parameters, white matter, and cerebrospinal fluid time series were fed into general linear models for nuisance regression to remove unwanted effects. Band-pass filtering (0.01 Hz-0.1 Hz) was performed to reduce low-frequency drift effects and high-frequency physiological noise for each subject. The resulting images were further spatially smoothed with full width at half maximum set at 0.8 mm. The region-to-region functional connectivity method was performed in this study to measure the correlations in spontaneous BOLD fluctuations. A network is comprised of nodes and edges; nodes being the brain region of interest (ROI) and edges being the connections between regions. Voxel time series data were averaged in each node based on the residual images using the nuisance regression procedure with motion parameters and mean time courses of white matter and ventricles. While there are 171 segmented brain regions in the rat brain atlas, this number (N) was reduced to 166. To acquire regional temporal correlations, Pearson's correlation coefficients were measured among (N * (N-1))/2 region pairs. For statistical inference on significant correlation, FDR (q=0.1) was applied for multiple correction. Pearson's correlation coefficients across all pairs of nodes (13695 pairs) were computed for each subject among all three groups to assess the interregional temporal correlations. The R-values (ranging from -1 to 1) were z-transformed using the Fisher's Z transform to improve normality. 166×166 symmetric connectivity matrices were constructed with each entry representing the strength of edge. Group-level analysis was performed to look at the functional connectivity in all experimental groups. The resulting Z-score matrices from one-group t-tests (against 0) were clustered using the K-nearest neighbors (KNN) method to identify clusters of nodes that form resting state networks reordering the brain areas to give symmetrical correlation matrices. The KNN algorithm generates an automatic clustering solution which reorders the nodes based on the distance between edge information so that smaller clusters are formed along the diagonal line of the matrix. A Z-score threshold of $|Z|=2.3$ was applied to remove spurious or weak node connections for visualization purposes. $|Z|<2.3$ equates to $p<0.02145$ for two-tailed hypothesis (connectivity significantly greater or less than 0). With an uncorrected *P* value =0.001, an accepted threshold voxel-wise analysis, the corresponding Z is 3.09.

Graph theory analysis

Degree centrality: Degree centrality analysis quantifies the number of connections a specific node has to the overall network. Degree centrality is defined as:

$$C_D(j) = \sum_{j=1}^{n} A_{ij}$$

Where n is the number of rows in the matrix in the adjacency matrix A and the elements of the matrix are given by A_{ij}, the number of edges between nodes i and j.

Table 1. Voxel based morphometry

Volumes (mm^3)					
	Veh	MPH	AMP		
Brain Area	Med	Med	Med	*P* Val	ω Sq
dentate n. cerebellum	0.78	1.32	0.78	0.001	0.578
pontine reticular nucleus	15.36	15.78	11.84	0.001	0.514
1st cerebellar lobule	1.36	1.73	1.09	0.002	0.474
primary somatosensory ctx shoulder	3.68	3.16	2.98	0.005	0.375
interposed n. cerebellum	1.23	1.87	1.34	0.011	0.310
perirhinal ctx	14.60	13.40	13.59	0.020	0.257
superior colliculus	20.08	19.24	15.24	0.021	0.251
claustrum	6.93	6.71	7.36	0.025	0.235
intercalated amygdala	0.91	0.80	0.81	0.030	0.221
CA1 hippocampus ventral	9.00	6.65	7.71	0.031	0.217
vestibular nucleus	9.78	10.80	9.90	0.034	0.209
parietal ctx	10.69	9.47	11.01	0.037	0.203
4th cerebellar lobule	17.22	15.02	14.40	0.037	0.202
suprachiasmatic nucleus	0.18	0.17	0.24	0.047	0.181

Statistics

All statistical analysis for the graph theory analysis was performed using GraphPad Prism version 9.0.0 (86) for macOS, GraphPad Software, San Diego, California USA, www.graphpad.com. Normality tests between group subregions were performed to determine if parametric or non-parametric assumptions were needed. Shapiro-Wilk's tests were performed to analyze normality assumption. Subregion degree centrality *P*-values greater than 0.05 were assumed to be normal. After assumptions of normality were validated, paired t-tests were used to compare degree centrality of the CBD and vehicle groups in various subregions. When necessary, a nonparametric Wilcoxon signed rank (WSR) test was performed if there was evidence against the normality assumption. Differences in degree between AMP, MPH and vehicle were visualized using Gephi software. Nodes that had a lower degree centrality in drug treatment versus vehicle were colored red.

Results

Voxel-based morphometry

Shown in **Table 1** are volumetric measures of different brain areas following 21 days of vehicle, MPH or AMP treatment. The median volume for each, together with a *P*-value and effect size is ranked in order of their significance. Only 14 out of 171 brain areas taken from the 3D MRI rat atlas showed significant differences using a critical value of 0.05. When corrected for FDR (P=0.016) and effect size (>0.3), only the first five are worth noting. Three of these five are associated with the cerebellum. It should be noted that both the dentate and interposed nuclei increased in volume with MPH treatment as compared to vehicle and AMP.

Diffusion weighted imaging

Shown in **Table 2** are data from DWI. The median values for each index of anisotropy are reported together with *P* values and effect size. Brain areas are ranked in order of significance, using a critical value of <0.05 as a threshold. No significant differences were found in linear diffusivity. When adjusting for multiple comparisons (FDR P=0.009) and a moderate effect size (>0.3), the only area of interest for FA is the lateral geniculate. Correcting for FDR leaves no significant differences in RD or ADC. Each area had AMP values higher and MPH values lower than vehicle.

Functional connectivity

Shown to the left of **Figure 1** are tables listing brains areas functionally coupled to the PFC for each of the three experimental treatments. The areas comprising the PFC, highlighted in red, were identified using a KNN clustering algorithm (see Z matrices for each treatment in Supplementary Table 1) and include the frontal association, ventral orbital, lateral orbital, prelimbic and infralimbic cortices. The values to the right show the average Z score for each brain area. In parentheses are the number of areas in the PFC significantly connected to that brain area that contributed to the average score. For example, the medial orbital cortex has significant connectivity with all five areas of the PFC as shown in the parentheses, and the average of the Z values for the medial orbital cortex is 2.88. Note that all the areas comprising the PFC are strongly coupled to each other. With vehicle treatment, there were

Table 2. Diffusion weighted imaging

Fractional Anisotropy					
	Veh	MPH	AMP		
Brain Area	Med	Med	Med	*P* Val	ω Sq
lateral geniculate	0.30	0.36	0.37	0.004	0.323
temporal ctx	0.32	0.37	0.35	0.009	0.267
inferior colliculus	0.30	0.36	0.39	0.023	0.201
paraventricular nucleus	0.34	0.41	0.41	0.028	0.185
superior colliculus	0.30	0.36	0.38	0.029	0.182
habenula nucleus	0.32	0.38	0.36	0.032	0.177
medial pretectal area	0.30	0.41	0.32	0.032	0.176
ectorhinal ctx	0.33	0.35	0.37	0.037	0.166
Apparent Diffusion Coefficient					
Brain Area	Med	Med	Med	*P* Val	ω Sq
supraoptic nucleus	2.78	2.38	3.14	0.039	0.161
Radial Diffusivity					
Brain Area	Med	Med	Med	*P* Val	ω Sq
supraoptic nucleus	0.70	0.61	0.76	0.003	0.345
magnocellular preoptic nucleus	0.66	0.60	0.81	0.017	0.224
pineal gland	1.15	0.78	0.88	0.032	0.175

15 areas positively correlated with the PFC. This connectivity includes parts of the olfactory system (glomerulus, anterior olfactory n., endopiriform ctx), forebrain cortex (medial orbital, primary and secondary motor, anterior cingulate, and somatosensory cortices) and the basal ganglia (accumbens, ventral striatum, septum). The organization of these areas with respect to the PFC can be seen in the 3D reconstructions to the right. The red represents the volume of the entire PFC, while the dark blue is the sensorimotor and forebrain cortical areas, the light blue is the olfactory system, and the yellow is the basal ganglia. In stark contrast to vehicle, treatment with MPH reduced the internal connectivity of the PFC, in addition to much of the forebrain ctx and all the basal ganglia. This dramatic loss of connectivity, as compared to vehicle, was also present after AMP treatment. The 3D reconstructions clearly show the reduction in connectivity with the PFC following 21 days of psychostimulant treatment.

Figure 2 shows the connectivity between the nodes of the PFC highlighted as black circles and brain areas comprising the basal ganglia (inner circle) and cerebral cortex (outer circle). The small circles highlighted in red denote specific brain areas that have significantly fewer degrees, or connections to the PFC nodes. The gray circle denoting the medial orbital cortex was not significantly different from the PFC. **Figure 3** shows bar graphs that summarize the difference in connectivity between each of the experimental conditions for the basal ganglia, PFC, and sensorimotor cortex. In all cases, treatment with AMP or MPH produced significantly less coupling within these brain regions as compared to vehicle.

Figure 4 is bar graphs comparing connectivity in degrees between the different major brain regions and the cerebellum for each of the experimental conditions. The individual brain areas that make up these brain regions are provided in Supplementary Table 2. The ARAS denotes the ascending reticular activating system. In all cases, except for the sensorimotor cortices, periadolescent rats treated with AMP showed a decoupling in connectivity as compared to vehicle and MPH. Indeed, it was only the sensorimotor cortices that were decoupled from the cerebellum for both psychostimulants as compared to vehicle. It is noteworthy that except for the sensorimotor cortices there were no significant differences in cerebellar connectivity between vehicle and MPH.

Behavioral testing

There were not significant treatment effects associated with behavioral testing in time spent with novel object as a percentage of total time with familiar and novel objects, total time spent with novel object, encounters with the novel object or distance traveled (**Figure 5**). All groups showed significant novel object interaction time compared to a predicted baseline of 50%.

Discussion

This study was undertaken to assess the effect of chronic psychostimulant exposure from the onset of juvenility through preadolescence on brain structure and function as indicated using multimodal MRI. The data show that MPH, the most used drug to treat ADHD, had few significant effects on brain volumes outside the cerebellum. DWI showed no differences in gray

Connections with the Prefrontal Cortex

Brain Areas in the Prefrontal Cortex
frontal association, ventral orbital, lateral orbital, prelimbic and infralimbic cortices

Vehicle		MPH		AMP	
Positive Correlation	Z score	Positive Correlation	Z score	Positive Correlation	Z score
frontal association ctx	2.76 (4)	frontal association ctx	NS	frontal association ctx	NS
ventral orbital ctx	3.17 (4)	ventral orbital ctx	NS	ventral orbital ctx	NS
lateral orbital ctx	3.05 (4)	lateral orbital ctx	2.76	lateral orbital ctx	3.91 (4)
prelimbic ctx	2.99 (4)	prelimbic ctx	NS	prelimbic ctx	NS
infralimbic ctx	2.93 (4)	infralimbic ctx	NS	infralimbic ctx	NS
medial orbital ctx	2.88 (5)	medial orbital ctx	3.44 (4)	medial orbital ctx	3.44 (4)
endopiriform ctx	3.18 (4)	claustrum	3.18 (4)	anterior olfactory n.	2.71 (5)
primary motor ctx	2.78 (5)	somatosensory ctx, jaw	3.08 (4)	insular ctx	2.92 (4)
secondary motor ctx	3.27 (5)	glomerular layer, bulb	3.24 (4)		
anterior cingulate ctx	2.73 (4)	granular layer, bulb	2.77 (4)		
insular ctx	2.94 (4)				
somatosensory ctx, jaw	3.07 (4)				
somatosensory ctx, forelimb	2.63 (5)				
claustrum	2.26 (4)				
glomerular layer, bulb	2.69 (5)				
anterior olfactory n.	2.94 (5)				
accumbens core	2.88 (5)				
accumbens shell	2.78 (5)				
ventral medial striatum	2.83 (5)				
lateral septum	2.83 (4)				

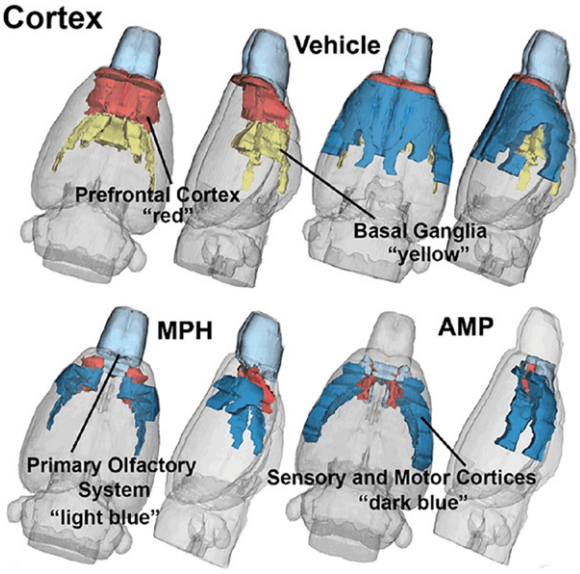

Figure 1. Functional coupling with the prefrontal cortex. Shown in the tables highlighted in red are the brain areas that comprise the prefrontal cortex. Below each is a list of brain areas with significant connections (Z values) to these areas for each of the experimental conditions. While all areas that comprise the PFC are interconnected with vehicle treatment, all but the lateral orbital ctx is not significantly coupled (NS) with MPH or AMP. The 3D reconstructions on the right provide an illustrated summary of the data on the left.

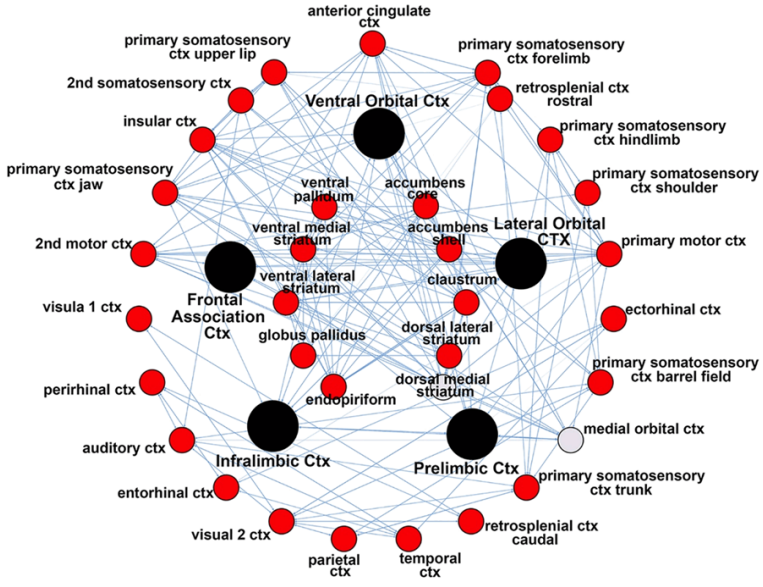

Figure 2. Connectivity between nodes. The radial figure shows the connectivity between the nodes of the PFC highlighted as black circles and brain areas comprising the basal ganglia (inner circle) and cerebral cortex (outer circle). Circles highlighted in red denote specific brain areas that have significantly fewer degrees or connections to the PFC nodes. The gray circle denoting the medial orbital cortex was not significantly different from the PFC.

matter microarchitecture, a proxy for brain injury [58]. Our initial hypothesis predicted an increase in coupling in the PFC under MPH treatment. Instead, we found decreased coupling in the PFC/basal ganglia/sensory-motor neural circuits. Our findings are discussed in the context of the clinical literature.

The PFC has been a major focus of ADHD research [59, 60]. Its prominence is supported by preclinical and clinical studies detailing its delayed developmental maturation in adolescence [61, 62], dopaminergic regulation [63], and its function in goal-directed and self-regulatory behavior [14, 64]. Patients diagnoses with ADHD show altered PFC structure [11] and function [65, 66] and enhanced activity to MPH during cognitive tasks [12, 13, 67-69]. We were surprised to find that peri-adolescent rats exposed to MPH showed pronounced decoupling of the PFC. This was not unique to the drug or dose, as AMP treatment showed similar results. Hence, the effect was common to two psychostimulants used to affect PFC function. Vehicle treated

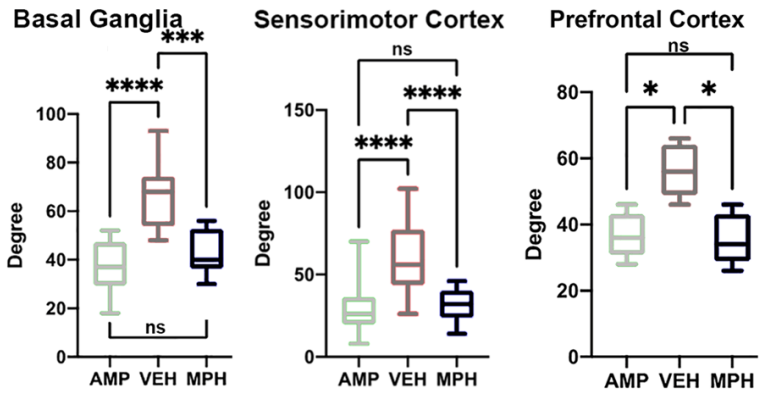

Figure 3. Degrees of connectivity between basal ganglia, prefrontal cortex, and sensorimotor cortex. The bar graphs summarize the difference in connectivity by degrees for each brain region for each of the experimental conditions. *P<0.05; ***P<0.001; ****P<0.0001.

rats showed the expected coupling between the PFC and striatum (see **Figure 1**), corroborating the PFC-striatal model of connectivity [70]. While the results were unexpected there is evidence from preclinical or clinical studies to support these findings. Chronic treatment of low dose (1 mg/kg) MPH suppresses neural activity in the PFC of "normal" juvenile rats that recovers within 1 week following cessation of treatment. While treatment with a higher dose (9 mg/kg) depresses activity for months [71]. A study by Farr and coworkers reported that a single oral dose of MPH in healthy adults reduced PFC connectivity [72]. It was proposed that clinical populations, i.e., ADHD with compromised DA neurotransmission show an increase in PFC activity to MPH while healthy subject will present with a dampened response caused by DA release exceeding its optimal level. For ethical reasons there have been no longitudinal studies giving MPH or AMP to normal peri-adolescent children.

It is possible that the changes in PFC coupling, increases or decreases, are unrelated to the efficacy of psychostimulant treatment. A meta-analysis of fMRI studies found mixed results regarding ADHD treatment-related alterations in the PFC. Some studies found no alterations in PFC activity in medicated vs. control groups, other studies found attenuated differences, while still others found augmented differences in PFC activity after treatment [32]. A recent study by Tremblay and coworkers measured the effects of MPH on cognitive behavior in rhesus monkeys while simultaneously recording electrical activity from the PFC and showed no correlation between the behavior and electrophysiology, leading them to suggest that MPH improves cognitive performance by acting on other areas of the brain [73]. The decoupling of the PFC/basal ganglia/sensory-motor neural circuitry found in our study with chronic MPH treatment does not support a role for the PFC in the etiology of ADHD or its treatment. To this point, a study by Hong et al., reported a significant reduction in connectivity between the basal ganglia, i.e., caudate/putamen/accumbens and the orbital frontal gyri, frontal cortices, anterior cingulate, and insular ctx in ADHD children that responded positively to MPH treatment [74]. The original model of fronto-striatal circuits in ADHD has been expanded to include a more global set of interconnected neural networks with an emphasis on the cerebellum. The cerebellum, aside from its role in motor coordination, also functions in attention, memory, and emotional processing [75]. These functions arise from a closed loop circuits between the cerebrum, basal ganglia, and the cerebellum [76].

Durston and colleagues proposed that dysfunction in the fronto-cerebellar circuits may contribute to the pathophysiology of ADHD due to its sexually dimorphic development and susceptibility to environmental influences and reported that chronic MPH treatment can normalize fronto-striatal-cerebellar circuits in children with ADHD [77]. Other studies have also pointed to the cerebellum as having a role in the pathology of ADHD [28, 32, 68]. Dysfunction of the cerebellum has been associated with symptoms similar to ADHD [78]. Kucyi et al., reported impaired connectivity between the cerebellum and default mode network in ADHD subjects as compared to controls [79]. Our studies show that chronic exposure to MPH throughout preadolescence increases the size of the deep cerebellar nuclei, the primary origin of efferent information coming from the cerebellum, while not affecting cerebellar connectivity to major brain regions ex-

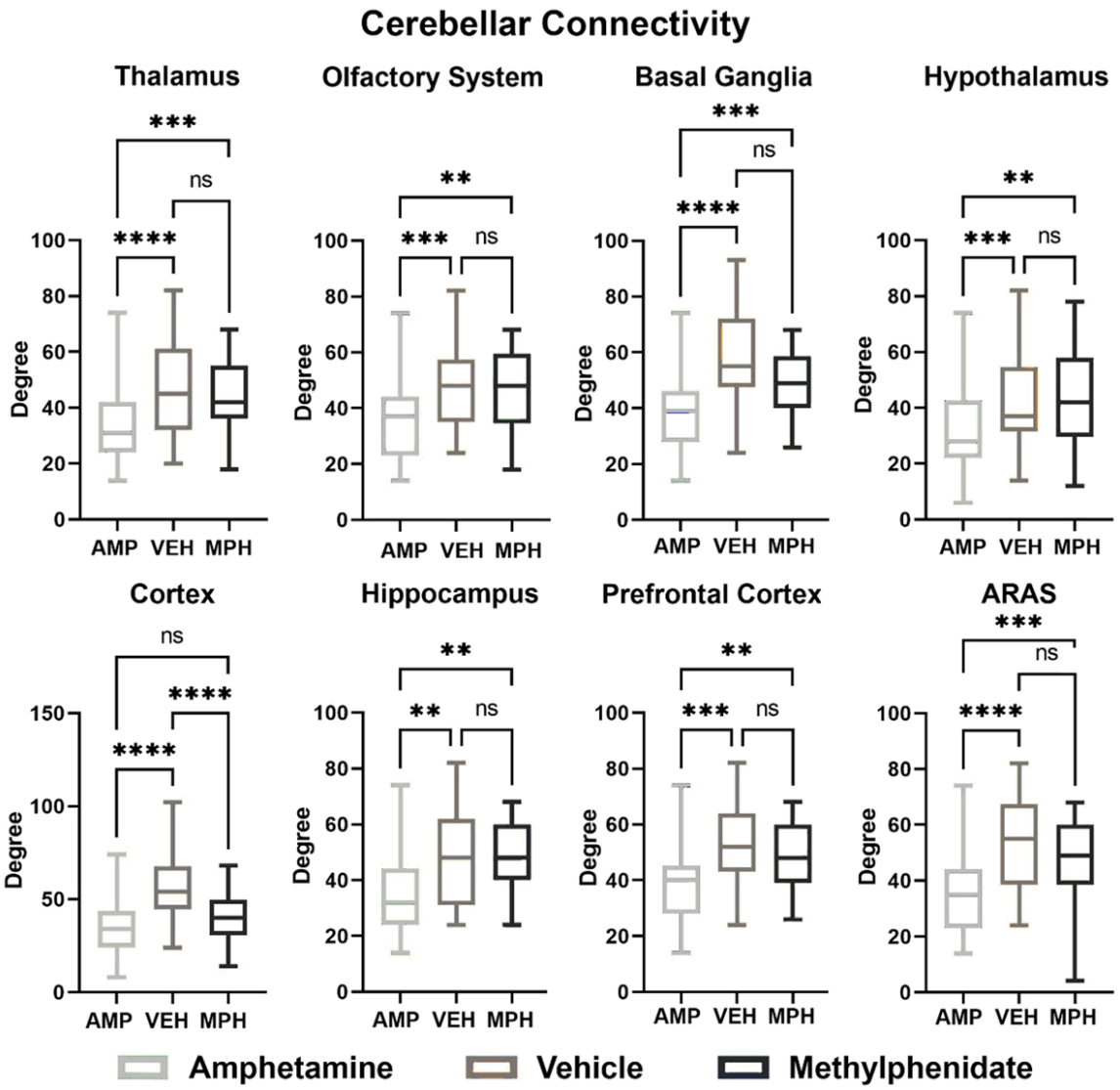

Figure 4. Functional coupling to the cerebellum. Shown are bar graphs comparing connectivity in degrees between the different major brain regions and the cerebellum for each of the experimental conditions. ARAS-ascending reticular activating system. *P<0.05; **P<0.01; ***P<0.001.

cept for the sensorimotor cortices and pons. These changes may reflect a shift in default brain circuitry away from typical networks and towards a more cerebellum-centered network following chronic MPH exposure. Interestingly, rats with a history of periadolescent exposure to AMP resulted in a general decrease in connectivity between the cerebellum and all other major brain regions.

In our study, there were very few brain areas that showed changes in volume to chronic exposure to MPH. These changes were primarily confined to the cerebellum, e.g., cerebellar nuclei and 1st cerebellar lobule. Structural MRI studies on children and adolescents with genetic risk and diagnosed with ADHD report a general decrease in intracranial volumes in the areas of accumbens, striatum, amygdala, hippocampus and cerebellum as compared with controls [80, 81]. There are reports that treatment with psychostimulants may normalize the trajectory of cortical development in ADHD [82]. Studies show morphological differences between psychostimulant-treatment naïve and chronically treated children with ADHD, specifically in regions involved in cognition [68, 83, 84]. Imaging studies have shown that ADHD patients medicated with MPH and/or AMP were found to have brain structures that were

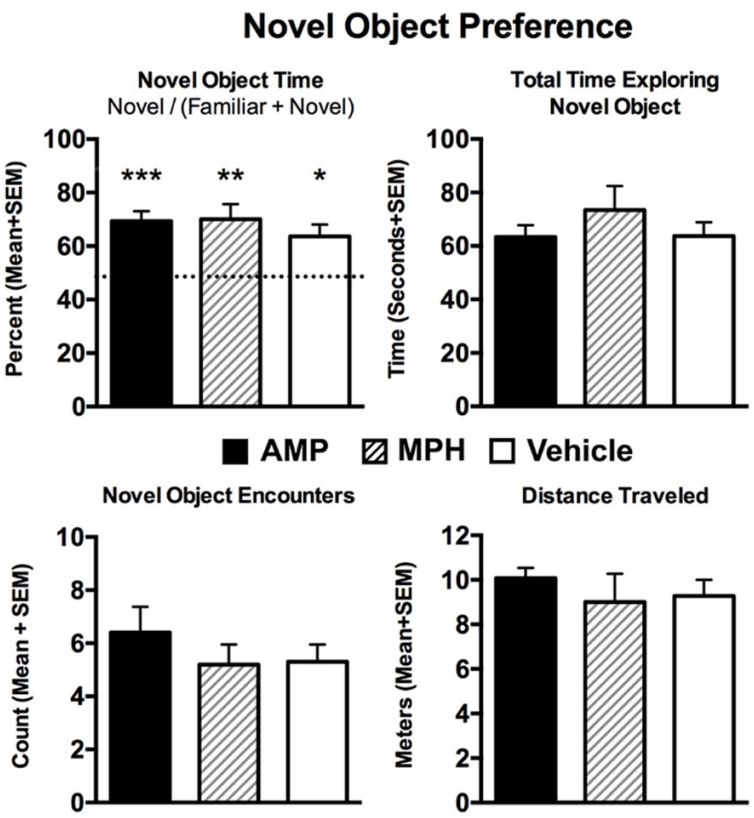

Figure 5. Novel object preference. Shown are average measures of performance collected in the novel object preference tests under the three experimental conditions. The first bar graph shows percentage of time spent with the novel object, the second total time exploring the novel object, the third encounters with it, and the fourth distance traveled. One-way ANOVA showed no significant differences between experimental groups for each measure as noted beneath each bar graph. A one sample t-test with a theoretical mean of 0.5 showed that each experiment group spent significantly more time in the novel environment. ***P<0.001, **P<0.01, *P<0.05.

generally more like non-ADHD controls than they were to unmedicated ADHD patients [32]. However, these finding are equivocal, as others report differences in brain volumes persist between treated and non-treated including the PFC [11]. Again, for ethical reasons, there have been no longitudinal studies on normal children looking at changes in brain structure in response to chronic exposure to MPH.

Limitations

These studies did not include a rodent model of ADHD. One might contend that our novel finding is unique to the "normal" Sprague Dawley rat. However, this seems relatively unlikely as the neurobiology of PFC and cerebellum should not be so distinct from phenotypic models of ADHD, e.g., SH rat [85] or humans, nor should "normal" be considered an anomaly. Indeed, we hypothesize that all mammals would present with a similar neuroradiological fingerprint when treated continuously throughout preadolescence with the doses of MPH or AMP as reported here.

Another limitation to this study was the absence of dose-dependent data. Many preclinical studies use doses designed to mimic blood levels achieved with oral dosing in ADHD patients. Those treatments include 2 mg/kg twice daily [15] as opposed to the 10 mg/kg given as a single dose in this study. Indeed, the pronounced decrease in cerebellar functional connectivity to all brain regions was only observed with AMP and not MPH. This comparison could have been different if explored across a range of doses. Additionally, we excluded female animals from our study. As an exploratory study, we chose male animals, because ADHD- and subsequently MPH usage- is more prevalent in boys than in girls [2]. Another important limitation is that we did not perform any behavioral assay that relates to frontal lobe function. Our behavioral analysis was limited to a single hippocampal memory task, novel object preference for which there were no significant differences. Additionally, rsFC was collected while rats were lightly anesthetized with isoflurane to minimize motion and physiological stress during "resting state" BOLD functional connectivity imaging (Review see [86]). Anesthesia may reduce the magnitude of the BOLD signal but does not disrupt the connectivity as demonstrated across species and under different physiological conditions [87-91]. Finally, we did not perform any postmortem histology that may have provided a better understanding of the cellular and neurochemical changes that occurred in the PFC and deep cerebellar nuclei.

Conclusion

In this study we report that chronic MPH exposure during periadolescent development results in decoupling of the wild-type rat PFC/basal ganglia/sensory-motor neural circuits while maintaining cerebellar connectivity to much of the brain. It is important to note that these functional changes did not manifest in any behavioral changes in NOP assay. These findings suggest that the MPH-induced alterations in brain function during preadolescence may shift the influence away from prefrontal regions to the cerebellum.

Acknowledgements

Dr. Amy E. Wagler for her mentorship in graph theory methods. Support for this study was provided in part by the Larry P. Jones Distinguished Professorship Endowment through The University of Texas El Paso (BSC), NIH MIGMS 5R25GM069621-17 (RJO). Support provided in part by a HHMI funded Inclusive Excellence Award to Northeastern University PI Ondrechen.

Disclosure of conflict of interest

Craig Ferris has a financial interest in Animal Imaging Research, the company that makes the radiofrequency electronics and holders for animal imaging.

Abbreviations

PFC, prefrontal cortex; NOP, novel object preference; MPH, methylphenidate; AMP, dextroamphetamine; DA, dopamine; NE, norepinephrine; MRI, magnetic resonance imaging; DWI, diffusion weighted imaging; VBM, voxel-based morphometry; PND, postnatal day; FA, fractional anisotropy; ADC, apparent diffusion coefficient; RD, radial diffusivity; L1, linear diffusivity; RARE, rapid acquisition relaxation enhanced; TE, echo time; TR, repetition time; EPI, echo planar imaging.

Address correspondence to: Craig Ferris, Department of Psychology, Northeastern University, 125 NI Hall, 360 Huntington Ave, Boston, MA 02115-5000, USA. Tel: 508-259-4908; E-mail: c.ferris@northeastern.edu

References

[1] American Psychiatric Association. Neurodevelopmental Disorders. Diagnostic and statistical manual of mental disorders. 5th edition. Washinton, DC: American Psychiatric Association Publishing; 2013.

[2] Danielson ML, Bitsko RH, Ghandour RM, Holbrook JR, Kogan MD and Blumberg SJ. Prevalence of parent-reported ADHD diagnosis and associated treatment among U.S. children and adolescents, 2016. J Clin Child Adolesc Psychol 2018; 47: 199-212.

[3] Bruchmuller K, Margraf J and Schneider S. Is ADHD diagnosed in accord with diagnostic criteria? Overdiagnosis and influence of client gender on diagnosis. J Consult Clin Psychol 2012; 80: 128-38.

[4] Ford-Jones PC. Misdiagnosis of attention deficit hyperactivity disorder: 'Normal behaviour' and relative maturity. Paediatr Child Health 2015; 20: 200-2.

[5] Thomas R, Sanders S, Doust J, Beller E and Glasziou P. Prevalence of attention-deficit/hyperactivity disorder: a systematic review and meta-analysis. Pediatrics 2015; 135: e994-1001.

[6] Spear LP. The adolescent brain and age-related behavioral manifestations. Neurosci Biobehav Rev 2000; 24: 417-63.

[7] Sowell ER, Trauner DA, Gamst A and Jernigan TL. Development of cortical and subcortical brain structures in childhood and adolescence: a structural MRI study. Dev Med Child Neurol 2002; 44: 4-16.

[8] Faraone SV, Asherson P, Banaschewski T, Biederman J, Buitelaar JK, Ramos-Quiroga JA, Rohde LA, Sonuga-Barke EJ, Tannock R and Franke B. Attention-deficit/hyperactivity disorder. Nat Rev Dis Primers 2015; 1: 15020.

[9] Berridge CW, Devilbiss DM, Andrzejewski ME, Arnsten AF, Kelley AE, Schmeichel B, Hamilton C and Spencer RC. Methylphenidate preferentially increases catecholamine neurotransmission within the prefrontal cortex at low doses that enhance cognitive function. Biol Psychiatry 2006; 60: 1111-1120.

[10] Del Campo N, Chamberlain SR, Sahakian BJ and Robbins TW. The roles of dopamine and noradrenaline in the pathophysiology and treatment of attention-deficit/hyperactivity disorder. Biol Psychiatry 2011; 69: e145-57.

[11] Seidman LJ, Valera EM and Makris N. Structural brain imaging of attention-deficit/hyperactivity disorder. Biol Psychiatry 2005; 57: 1263-72.

[12] Spencer RC, Devilbiss DM and Berridge CW. The cognition-enhancing effects of psychostimulants involve direct action in the prefrontal cortex. Biol Psychiatry 2015; 77: 940-50.

[13] Zang YF, Jin Z, Weng XC, Zhang L, Zeng YW, Yang L, Wang YF, Seidman LJ and Faraone SV. Functional MRI in attention-deficit hyperactivi-

ty disorder: evidence for hypofrontality. Brain Dev 2005; 27: 544-50.
[14] Casey BJ, Giedd JN and Thomas KM. Structural and functional brain development and its relation to cognitive development. Biol Psychol 2000; 54: 241-57.
[15] Andersen SL, Arvanitogiannis A, Pliakas AM, LeBlanc C and Carlezon WA Jr. Altered responsiveness to cocaine in rats exposed to methylphenidate during development. Nat Neurosci 2002; 5: 13-4.
[16] Carlezon WA Jr, Mague SD and Andersen SL. Enduring behavioral effects of early exposure to methylphenidate in rats. Biol Psychiatry 2003; 54: 1330-7.
[17] Bolanos CA, Barrot M, Berton O, Wallace-Black D and Nestler EJ. Methylphenidate treatment during pre- and periadolescence alters behavioral responses to emotional stimuli at adulthood. Biol Psychiatry 2003; 54: 1317-29.
[18] Pardey MC, Kumar NN, Goodchild AK, Clemens KJ, Homewood J and Cornish JL. Long-term effects of chronic oral Ritalin administration on cognitive and neural development in adolescent wistar kyoto rats. Brain Sci 2012; 2: 375-404.
[19] Crawford CA, Baella SA, Farley CM, Herbert MS, Horn LR, Campbell RH and Zavala AR. Early methylphenidate exposure enhances cocaine self-administration but not cocaine-induced conditioned place preference in young adult rats. Psychopharmacology (Berl) 2011; 213: 43-52.
[20] Adriani W, Leo D, Greco D, Rea M, di Porzio U, Laviola G and Perrone-Capano C. Methylphenidate administration to adolescent rats determines plastic changes on reward-related behavior and striatal gene expression. Neuropsychopharmacology 2006; 31: 1946-56.
[21] Achat-Mendes C, Anderson KL and Itzhak Y. Methylphenidate and MDMA adolescent exposure in mice: long-lasting consequences on cocaine-induced reward and psychomotor stimulation in adulthood. Neuropharmacology 2003; 45: 106-15.
[22] Yang PB, Swann AC and Dafny N. Acute and chronic methylphenidate dose-response assessment on three adolescent male rat strains. Brain Res Bull 2006; 71: 301-10.
[23] Abbas Z, Sweet A, Hernandez G and Arvanitogiannis A. Adolescent exposure to methylphenidate increases impulsive choice later in life. Front Behav Neurosci 2017; 11: 214.
[24] Rowan JD, McCarty MK, Kundey SM, Osburn CD, Renaud SM, Kelley BM, Matoushek AW and Fountain SB. Adolescent exposure to methylphenidate impairs serial pattern learning in the serial multiple choice (SMC) task in adult rats. Neurotoxicol Teratol 2015; 51: 21-6.
[25] Halladay LR, Iniguez SD, Furqan F, Previte MC, Chisum AM and Crawford CA. Methylphenidate potentiates morphine-induced antinociception, hyperthermia, and locomotor activity in young adult rats. Pharmacol Biochem Behav 2009; 92: 190-6.
[26] Venkataraman SS, Joseph M and Dafny N. Concomitant behavioral and prefrontal cortex neuronal responses following acute and chronic methylphenidate exposure in adolescent and adult rats. Brain Res Bull 2019; 144: 200-212.
[27] Schmitz F, Pierozan P, Rodrigues AF, Biasibetti H, Grunevald M, Pettenuzzo LF, Scaini G, Streck EL, Netto CA and Wyse ATS. Methylphenidate causes behavioral impairments and neuron and astrocyte loss in the hippocampus of juvenile rats. Mol Neurobiol 2017; 54: 4201-4216.
[28] Soto PL, Wilcox KM, Zhou Y, Kumar A, Ator NA, Riddle MA, Wong DF and Weed MR. Long-term exposure to oral methylphenidate or dl-amphetamine mixture in peri-adolescent rhesus monkeys: effects on physiology, behavior, and dopamine system development. Neuropsychopharmacology 2012; 37: 2566-79.
[29] Arnsten AF. Stimulants: therapeutic actions in ADHD. Neuropsychopharmacology 2006; 31: 2376-83.
[30] Castellanos FX and Aoki Y. Intrinsic functional connectivity in attention-deficit/hyperactivity disorder: a science in development. Biol Psychiatry Cogn Neurosci Neuroimaging 2016; 1: 253-261.
[31] Thompson PM, Andreassen OA, Arias-Vasquez A, Bearden CE, Boedhoe PS, Brouwer RM, Buckner RL, Buitelaar JK, Bulayeva KB, Cannon DM, Cohen RA, Conrod PJ, Dale AM, Deary IJ, Dennis EL, de Reus MA, Desrivieres S, Dima D, Donohoe G, Fisher SE, Fouche JP, Francks C, Frangou S, Franke B, Ganjgahi H, Garavan H, Glahn DC, Grabe HJ, Guadalupe T, Gutman BA, Hashimoto R, Hibar DP, Holland D, Hoogman M, Pol HEH, Hosten N, Jahanshad N, Kelly S, Kochunov P, Kremen WS, Lee PH, Mackey S, Martin NG, Mazoyer B, McDonald C, Medland SE, Morey RA, Nichols TE, Paus T, Pausova Z, Schmaal L, Schumann G, Shen L, Sisodiya SM, Smit DJA, Smoller JW, Stein DJ, Stein JL, Toro R, Turner JA, van den Heuvel MP, van den Heuvel OL, van Erp TGM, van Rooij D, Veltman DJ, Walter H, Wang Y, Wardlaw JM, Whelan CD, Wright MJ and Ye J; ENIGMA Consortium. ENIGMA and the individual: predicting factors that affect the brain in 35 countries worldwide. Neuroimage 2017; 145: 389-408.
[32] Spencer TJ, Brown A, Seidman LJ, Valera EM, Makris N, Lomedico A, Faraone SV and Biederman J. Effect of psychostimulants on brain structure and function in ADHD: a qualitative literature review of magnetic resonance imaging-based neuroimaging studies. J Clin Psychiatry 2013; 74: 902-17.

[33] Kilkenny C, Browne WJ, Cuthill IC, Emerson M and Altman DG. Improving bioscience research reporting: the ARRIVE guidelines for reporting animal research. PLoS Biol 2010; 8: e1000412.
[34] LeBlanc-Duchin D and Taukulis HK. Chronic oral methylphenidate administration to periadolescent rats yields prolonged impairment of memory for objects. Neurobiol Learn Mem 2007; 88: 312-20.
[35] Brandon CL, Marinelli M, Baker LK and White FJ. Enhanced reactivity and vulnerability to cocaine following methylphenidate treatment in adolescent rats. Neuropsychopharmacology 2001; 25: 651-61.
[36] Sherrill LK, Stanis JJ and Gulley JM. Age-dependent effects of repeated amphetamine exposure on working memory in rats. Behav Brain Res 2013; 242: 84-94.
[37] Santos GC, Marin MT, Cruz FC, Delucia R and Planeta CS. Amphetamine- and nicotine-induced cross-sensitization in adolescent rats persists until adulthood. Addict Biol 2009; 14: 270-5.
[38] Doremus-Fitzwater TL and Spear LP. Amphetamine-induced incentive sensitization of sign-tracking behavior in adolescent and adult female rats. Behav Neurosci 2011; 125: 661-7.
[39] Sherrill LK and Gulley JM. Effects of amphetamine exposure during adolescence on behavior and prelimbic cortex neuron activity in adulthood. Brain Res 2018; 1694: 111-120.
[40] Yetnikoff L, Pokinko M, Arvanitogiannis A and Flores C. Adolescence: a time of transition for the phenotype of dcc heterozygous mice. Psychopharmacology (Berl) 2014; 231: 1705-14.
[41] Sengupta P. The laboratory rat: relating its age with human's. Int J Prev Med 2013; 4: 624-30.
[42] Morrison TR, Kulkarni P, Cai X, Iriah S, Aggarwal D, Lu SF, Simon NG, Madularu D and Ferris CF. Treating head injury using a novel vasopressin 1a receptor antagonist. Neurosci Lett 2020; 714: 134565.
[43] Ferris CF, Cai X, Qiao J, Switzer B, Baun J, Morrison T, Iriah S, Madularu D, Sinkevicius KW and Kulkarni P. Life without a brain: neuroradiological and behavioral evidence of neuroplasticity necessary to sustain brain function in the face of severe hydrocephalus. Sci Rep 2019; 9: 16479.
[44] Madularu D, Kulkarni P, Ferris CF and Brake WG. Changes in brain volume in response to estradiol levels, amphetamine sensitization and haloperidol treatment in awake female rats. Brain Res 2015; 1618: 100-10.
[45] Cai X, Qiao J, Knox T, Iriah S, Kulkarni P, Madularu D, Morrison T, Waszczak B, Hartner JC and Ferris CF. In search of early neuroradiological biomarkers for Parkinson's disease: alterations in resting state functional connectivity and gray matter microarchitecture in PINK1-/- rats. Brain Res 2019; 1706: 58-67.
[46] Sinkevicius KW, Morrison TR, Kulkarni P, Caffrey Cagliostro MK, Iriah S, Malmberg S, Sabrick J, Honeycutt JA, Askew KL, Trivedi M and Ferris CF. RNaseT2 knockout rats exhibit hippocampal neuropathology and deficits in memory. Dis Model Mech 2018; 11: dmm032631.
[47] Ferris CF, Nodine S, Pottala T, Cai X, Knox TM, Fofana FH, Kim S, Kulkarni P, Crystal JD and Hohmann AG. Alterations in brain neurocircuitry following treatment with the chemotherapeutic agent paclitaxel in rats. Neurobiol Pain 2019; 6: 100034.
[48] Kulkarni P, Morrison TR, Cai X, Iriah S, Simon N, Sabrick J, Neuroth L and Ferris CF. Neuroradiological changes following single or repetitive mild TBI. Front Syst Neurosci 2019; 13: 34.
[49] Hoogenraad FG, Pouwels PJ, Hofman MB, Rombouts SA, Lavini C, Leach MO and Haacke EM. High-resolution segmented EPI in a motor task fMRI study. Magn Reson Imaging 2000; 18: 405-9.
[50] Kang D, Sung YW and Kang CK. Fast imaging technique for fMRI: consecutive multishot echo planar imaging accelerated with GRAPPA technique. Biomed Res Int 2015; 2015: 394213.
[51] Menon RS, Thomas CG and Gati JS. Investigation of BOLD contrast in fMRI using multi-shot EPI. NMR Biomed 1997; 10: 179-82.
[52] Poser BA and Norris DG. Investigating the benefits of multi-echo EPI for fMRI at 7 T. Neuroimage 2009; 45: 1162-72.
[53] Swisher JD, Sexton JA, Gatenby JC, Gore JC and Tong F. Multishot versus single-shot pulse sequences in very high field fMRI: a comparison using retinotopic mapping. PLoS One 2012; 7: e34626.
[54] Farzaneh F, Riederer SJ and Pelc NJ. Analysis of T2 limitations and off-resonance effects on spatial resolution and artifacts in echo-planar imaging. Magn Reson Med 1990; 14: 123-39.
[55] Jesmanowicz A, Bandettini PA and Hyde JS. Single-shot half k-space high-resolution gradient-recalled EPI for fMRI at 3 tesla. Magn Reson Med 1998; 40: 754-62.
[56] Benjamini Y and Hochberg Y. Controlling the false discovery rate: a practical and powerful approach to multiple testing. J R Stat Soc Series B Stat Methodol 1995; 57: 289-300.
[57] Honeycutt JA, Demaestri C, Peterzell S, Silveri MM, Cai X, Kulkarni P, Cunningham MG, Ferris CF and Brenhouse HC. Altered corticolimbic

connectivity reveals sex-specific adolescent outcomes in a rat model of early life adversity. Elife 2020; 9: e52651.
[58] Kulkarni P, Kenkel W, Finklestein SP, Barchet TM, Ren J, Davenport M, Shenton ME, Kikinis Z, Nedelman M and Ferris CF. Use of anisotropy, 3D segmented atlas, and computational analysis to identify gray matter subcortical lesions common to concussive injury from different sites on the cortex. PLoS One 2015; 10: e0125748.
[59] Casey BJ, Castellanos FX, Giedd JN, Marsh WL, Hamburger SD, Schubert AB, Vauss YC, Vaituzis AC, Dickstein DP, Sarfatti SE and Rapoport JL. Implication of right frontostriatal circuitry in response inhibition and attention-deficit/hyperactivity disorder. J Am Acad Child Adolesc Psychiatry 1997; 36: 374-83.
[60] Rubia K, Overmeyer S, Taylor E, Brammer M, Williams SC, Simmons A and Bullmore ET. Hypofrontality in attention deficit hyperactivity disorder during higher-order motor control: a study with functional MRI. Am J Psychiatry 1999; 156: 891-6.
[61] Casey BJ, Getz S and Galvan A. The adolescent brain. Dev Rev 2008; 28: 62-77.
[62] Caballero A, Granberg R and Tseng KY. Mechanisms contributing to prefrontal cortex maturation during adolescence. Neurosci Biobehav Rev 2016; 70: 4-12.
[63] Cools R, Frobose M, Aarts E and Hofmans L. Dopamine and the motivation of cognitive control. Handb Clin Neurol 2019; 163: 123-143.
[64] Romine CB and Reynolds CR. A model of the development of frontal lobe functioning: findings from a meta-analysis. Appl Neuropsychol 2005; 12: 190-201.
[65] Sheridan MA, Hinshaw S and D'Esposito M. Efficiency of the prefrontal cortex during working memory in attention-deficit/hyperactivity disorder. J Am Acad Child Adolesc Psychiatry 2007; 46: 1357-1366.
[66] Cheng W, Ji X, Zhang J and Feng J. Individual classification of ADHD patients by integrating multiscale neuroimaging markers and advanced pattern recognition techniques. Front Syst Neurosci 2012; 6: 58.
[67] Silk TJ, Malpas C, Vance A and Bellgrove MA. The effect of single-dose methylphenidate on resting-state network functional connectivity in ADHD. Brain Imaging Behav 2017; 11: 1422-1431.
[68] Rubia K, Halari R, Cubillo A, Mohammad AM, Brammer M and Taylor E. Methylphenidate normalises activation and functional connectivity deficits in attention and motivation networks in medication-naive children with ADHD during a rewarded continuous performance task. Neuropharmacology 2009; 57: 640-52.
[69] Rubia K, Halari R, Cubillo A, Smith AB, Mohammad AM, Brammer M and Taylor E. Methylphenidate normalizes fronto-striatal underactivation during interference inhibition in medication-naive boys with attention-deficit hyperactivity disorder. Neuropsychopharmacology 2011; 36: 1575-86.
[70] Castellanos FX and Proal E. Large-scale brain systems in ADHD: beyond the prefrontal-striatal model. Trends Cogn Sci 2012; 16: 17-26.
[71] Urban KR, Waterhouse BD and Gao WJ. Distinct age-dependent effects of methylphenidate on developing and adult prefrontal neurons. Biol Psychiatry 2012; 72: 880-8.
[72] Farr OM, Zhang S, Hu S, Matuskey D, Abdelghany O, Malison RT and Li CS. The effects of methylphenidate on resting-state striatal, thalamic and global functional connectivity in healthy adults. Int J Neuropsychopharmacol 2014; 17: 1177-91.
[73] Tremblay S, Pieper F, Sachs A, Joober R and Martinez-Trujillo J. The effects of methylphenidate (Ritalin) on the neurophysiology of the monkey caudal prefrontal cortex. eNeuro 2019; 6: ENEURO.0371-18.2018.
[74] Hong SB, Harrison BJ, Fornito A, Sohn CH, Song IC and Kim JW. Functional dysconnectivity of corticostriatal circuitry and differential response to methylphenidate in youth with attention-deficit/hyperactivity disorder. J Psychiatry Neurosci 2015; 40: 46-57.
[75] Strick PL, Dum RP and Fiez JA. Cerebellum and nonmotor function. Annu Rev Neurosci 2009; 32: 413-34.
[76] Schmahmann JD. The cerebellum and cognition. Neurosci Lett 2019; 688: 62-75.
[77] Durston S, van Belle J and de Zeeuw P. Differentiating frontostriatal and fronto-cerebellar circuits in attention-deficit/hyperactivity disorder. Biol Psychiatry 2011; 69: 1178-84.
[78] D'Angelo E and Casali S. Seeking a unified framework for cerebellar function and dysfunction: from circuit operations to cognition. Front Neural Circuits 2013; 6: 116.
[79] Kucyi A, Hove MJ, Biederman J, Van Dijk KR and Valera EM. Disrupted functional connectivity of cerebellar default network areas in attention-deficit/hyperactivity disorder. Hum Brain Mapp 2015; 36: 3373-86.
[80] Hoogman M, Bralten J, Hibar DP, Mennes M, Zwiers MP, Schweren LSJ, van Hulzen KJE, Medland SE, Shumskaya E, Jahanshad N, Zeeuw P, Szekely E, Sudre G, Wolfers T, Onnink AMH, Dammers JT, Mostert JC, Vives-Gilabert Y, Kohls G, Oberwelland E, Seitz J, Schulte-Rüther M, Ambrosino S, Doyle AE, Høvik MF, Dramsdahl M, Tamm L, van Erp TGM, Dale A, Schork A, Conzelmann A, Zierhut K, Baur R, McCarthy H, Yoncheva YN, Cubillo A, Chanti-

luke K, Mehta MA, Paloyelis Y, Hohmann S, Baumeister S, Bramati I, Mattos P, Tovar-Moll F, Douglas P, Banaschewski T, Brandeis D, Kuntsi J, Asherson P, Rubia K, Kelly C, Martino AD, Milham MP, Castellanos FX, Frodl T, Zentis M, Lesch KP, Reif A, Pauli P, Jernigan TL, Haavik J, Plessen KJ, Lundervold AJ, Hugdahl K, Seidman LJ, Biederman J, Rommelse N, Heslenfeld DJ, Hartman CA, Hoekstra PJ, Oosterlaan J, Polier GV, Konrad K, Vilarroya O, Ramos-Quiroga JA, Soliva JC, Durston S, Buitelaar JK, Faraone SV, Shaw P, Thompson PM and Franke B. Subcortical brain volume differences in participants with attention deficit hyperactivity disorder in children and adults: a cross-sectional mega-analysis. Lancet Psychiatry 2017; 4: 310-319.

[81] Mooney MA, Bhatt P, Hermosillo RJM, Ryabinin P, Nikolas M, Faraone SV, Fair DA, Wilmot B and Nigg JT. Smaller total brain volume but not subcortical structure volume related to common genetic risk for ADHD. Psychol Med 2020; [Epub ahead of print].

[82] Schweren LJ, de Zeeuw P and Durston S. MR imaging of the effects of methylphenidate on brain structure and function in attention-deficit/hyperactivity disorder. Eur Neuropsychopharmacol 2013; 23: 1151-64.

[83] Bledsoe J, Semrud-Clikeman M and Pliszka SR. A magnetic resonance imaging study of the cerebellar vermis in chronically treated and treatment-naive children with attention-deficit/hyperactivity disorder combined type. Biol Psychiatry 2009; 65: 620-4.

[84] Castellanos FX, Lee PP, Sharp W, Jeffries NO, Greenstein DK, Clasen LS, Blumenthal JD, James RS, Ebens CL, Walter JM, Zijdenbos A, Evans AC, Giedd JN and Rapoport JL. Developmental trajectories of brain volume abnormalities in children and adolescents with attention-deficit/hyperactivity disorder. JAMA 2002; 288: 1740-8.

[85] Sagvolden T, Johansen EB, Wøien G, Walaas SI, Storm-Mathisen J, Bergersen LH, Hvalby O, Jensen V, Aase H, Russell VA, Killeen PR, Dasbanerjee T, Middleton FA and Faraone SV. The spontaneously hypertensive rat model of AD-HD--the importance of selecting the appropriate reference strain. Neuropharmacology 2009; 57: 619-26.

[86] Gorges M, Roselli F, Muller HP, Ludolph AC, Rasche V and Kassubek J. Functional connectivity mapping in the animal model: principles and applications of resting-state fMRI. Front Neurol 2017; 8: 200.

[87] Liang Z, King J and Zhang N. Intrinsic organization of the anesthetized brain. J Neurosci 2012; 32: 10183-10191.

[88] Vincent JL, Patel GH, Fox MD, Snyder AZ, Baker JT, Van Essen DC, Zempel JM, Snyder LH, Corbetta M and Raichle ME. Intrinsic functional architecture in the anaesthetized monkey brain. Nature 2007; 447: 83-6.

[89] Gozzi A and Schwarz AJ. Large-scale functional connectivity networks in the rodent brain. Neuroimage 2016; 127: 496-509.

[90] Guilfoyle DN, Gerum SV, Sanchez JL, Balla A, Sershen H, Javitt DC and Hoptman MJ. Functional connectivity fMRI in mouse brain at 7T using isoflurane. J Neurosci Methods 2013; 214: 144-8.

[91] Jonckers E, Delgado y Palacios R, Shah D, Guglielmetti C, Verhoye M and Van der Linden A. Different anesthesia regimes modulate the functional connectivity outcome in mice. Magn Reson Med 2014; 72: 1103-12.

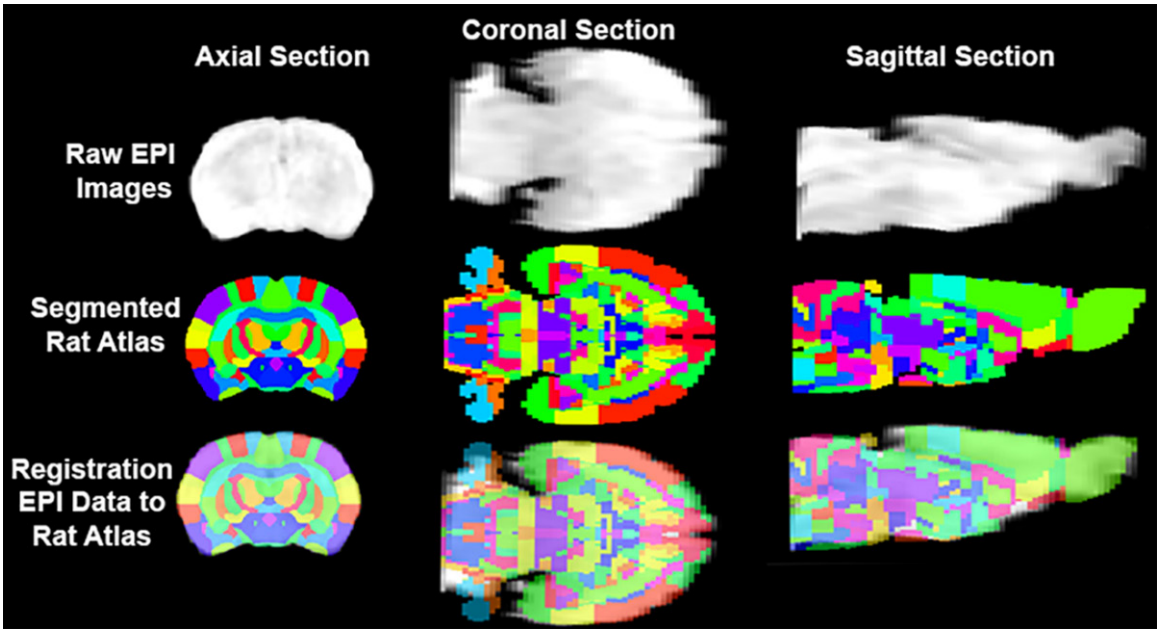

Figure S1. Neuroanatomical Fidelity. Shown are raw EPI images in different orthogonal directions and their registration of the segmented rat atlas.